Title
Genetic dissection reveals unexpected influence of β subunits on KCNQ1 K+ channel polarized trafficking in vivo

Journal
The FASEB Journal, 25(2)

ISSN
0892-6638

Authors
Roepke, Torsten K
King, Elizabeth C
Purtell, Kerry
et al.

Publication Date
2011-02-01

DOI
10.1096/fj.10-173682

Genetic dissection reveals unexpected influence of β subunits on KCNQ1 K^+ channel polarized trafficking *in vivo*

Torsten K. Roepke,[*,†,1,2] Elizabeth C. King,[*,1] Kerry Purtell,[*] Vikram A. Kanda,[*] Daniel J. Lerner,[†,3] and Geoffrey W. Abbott[*,†,4]

[*]Department of Pharmacology and [†]Department of Medicine, Weill Medical College of Cornell University, New York, New York, USA

ABSTRACT **Targeted deletion of the *Kcne2* potassium channel β subunit gene ablates gastric acid secretion and predisposes to gastric neoplasia in mice. Here, we discovered that *Kcne2* deletion basolaterally reroutes the Kcnq1 α subunit *in vivo* in parietal cells (PCs), in which the normally apical location of the Kcnq1–Kcne2 channel facilitates its essential role in gastric acid secretion. Quantitative RT-PCR and Western blotting revealed that *Kcne2* deletion remodeled fundic *Kcne3* (2.9±0.8-fold mRNA increase, *n*=10; 5.3±0.4-fold protein increase, *n*=7) but not *Kcne1*, *4*, or *5*, and resulted in basolateral Kcnq1–Kcne3 complex formation in $Kcne2^{-/-}$ PCs. Concomitant targeted deletion of *Kcne3* (creating $Kcne2^{-/-}Kcne3^{-/-}$ mice) restored PC apical Kcnq1 localization without *Kcne1*, *4*, or *5* remodeling (assessed by quantitative RT-PCR; *n*=5–10), indicating Kcne3 actively, basolaterally rerouted Kcnq1 in $Kcne2^{-/-}$ PCs. Despite this, *Kcne3* deletion exacerbated gastric hyperplasia in $Kcne2^{-/-}$ mice, and both hypochlorhydria and hyperplasia in $Kcne2^{+/-}$ mice, suggesting that Kcne3 up-regulation was beneficial in *Kcne2*-depleted PCs. The findings reveal, *in vivo*, Kcne-dependent α subunit polarized trafficking and the existence and consequences of potassium channel β subunit remodeling.—Roepke, T. K., King, E. C., Purtell, K., Kanda, V. A., Lerner, D. J., Abbott, G. W. Genetic dissection reveals unexpected influence of β subunits on KCNQ1 K^+ channel polarized trafficking *in vivo*. *FASEB J.* 25, 727–736 (2011). www.fasebj.org**

Key Words: gastric acid · MiRP1 · potassium channel

Parietal cells (PCs) achieve gastric acidification by virtue of an apical H^+/K^+ATPase (HKA) that pumps protons into the stomach lumen in exchange for K^+ ions. To maintain this activity, K^+ ions that enter the PC through the HKA must travel back into the stomach lumen across the apical membrane. This K^+ ion efflux occurs primarily through the heteromeric KCNQ1–KCNE2 K^+ channel (1, 2), with other K^+ channels also possibly contributing (3, 4). KCNQ1 is a 6-transmembrane segment (TMS) α subunit from the S4 superfamily that forms functional, voltage-gated, homotetrameric, K^+-selective channels in heterologous expression studies (5, 6). Originally named MinK-related peptide 1 (MiRP1), KCNE2 is a 1-TMS ancillary subunit from the *KCNE* gene family (7) (**Fig. 1*A***). Here, for simplicity, we will use the KCNE nomenclature to refer to both genes and proteins; as per convention, human protein names are written in uppercase, mouse in lowercase; genes are written the same but in italics; where no specific species is implied, we will use uppercase. All five known *KCNE* gene products have been shown to regulate KCNQ1 function in heterologous expression studies (8). Two of these—KCNE2 and KCNE3, originally named MiRP2 (7)—endow KCNQ1 with constitutive activation, probably by favoring the activated conformation of the KCNQ1 voltage sensor (9–11). While KCNE2 and KCNQ1 colocalize in the PC apical membrane (Fig. 1*B*), KCNQ1–KCNE3 channels target to the basolateral membrane of colonic epithelial cells, where they regulate cAMP-stimulated chloride secretion (10, 12, 13).

$Kcnq1^{-/-}$ mice and $Kcne2^{-/-}$ mice show similar gastric phenotypes, characterized by achlorhydria, hypergastrinemia, and gastric glandular hyperplasia (1, 2, 14). PCs from either null show ~10-fold reduced capacity to recover from proton loading, suggesting a primary defect in gastric acid secretion. The achlorhydria we previously observed in $Kcne2^{-/-}$ mice was striking given that Kcnq1, the pore-forming subunit of the complex, was still present, and in fact was strongly expressed in double the number of cells per gastric gland in $Kcne2^{-/-}$ mice compared to $Kcne2^{+/+}$ mice (2). PCs are nonexcitable, and their membrane potential reportedly varies from −20 to −40 mV, with stimulation by secretagogues such as gastrin, histamine, or carbachol causing a shift to the hyperpolarized end of

[1] These authors contributed equally to this work.

[2] Current address: Clinic for Cardiology and Angiology, Charité University-Medicine, Berlin, Campus Mitte and Experimental and Clinical Research Center, Max Delbrueck Center for Molecular Medicine, Berlin, Germany.

[3] Current address: Tyrx Inc., Monmouth Junction, NJ, USA.

[4] Correspondence: Department of Pharmacology, Weill Medical College of Cornell University, New York, NY 10021, USA. E-mail: gwa2001@med.cornell.edu

doi: 10.1096/fj.10-173682

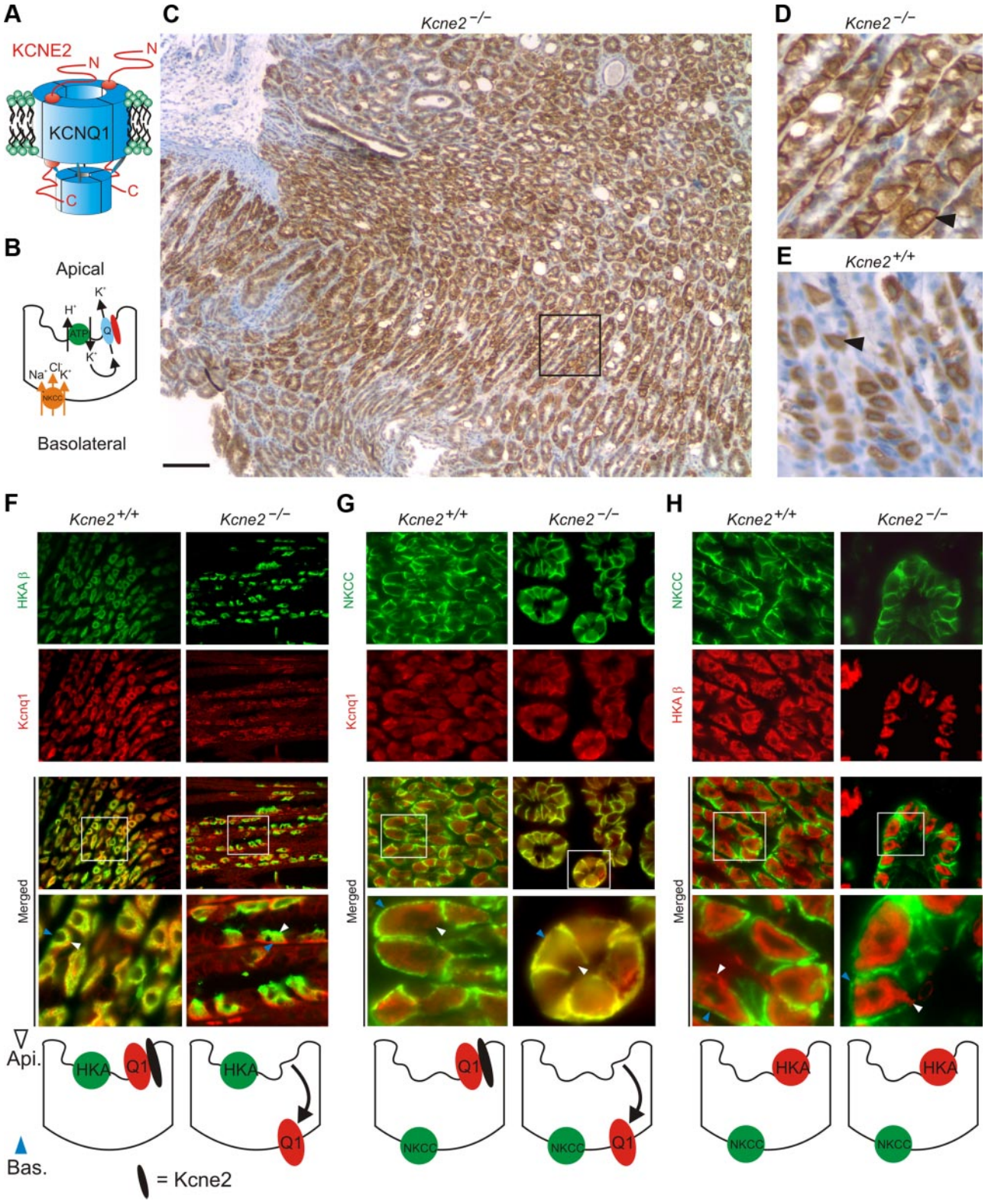

Figure 1. Reversed Kcnq1 trafficking in PCs of *Kcne2*$^{-/-}$ mice. *A*) Cartoon of a KCNQ1–KCNE2 complex. *B*) Cartoon of a PC showing location of HKA, NKCC1, and the KCNQ1–KCNE2 channel. *C*) KCNQ1 immunostaining (IS) in *Kcne2*$^{-/-}$ gastric mucosa. Scale bar = 100 μm. *D*) KCNQ1 IS in *Kcne2*$^{-/-}$ gastric mucosa (black box from panel *C*). Arrowhead indicates basolateral KCNQ1 staining. *E*) KCNQ1 IS in *Kcne2*$^{+/+}$ gastric mucosa (same scale as panel *D*). Arrowhead indicates diffuse KCNQ1 staining due to localization at the invaginated apical membrane. *F–H*) Top: exemplar IF colabeling of *Kcne2*$^{+/+}$ and *Kcne2*$^{-/-}$ gastric glands as indicated. "Merged" indicates merged view of the 2 panels above; bottom merged panel shows expanded view of the boxed region in the top merged panel. Yellow indicates colocalization. Blue arrowheads, PC basolateral side; white arrowheads, PC apical side. Representative of results from ≥2 mice, 3–5 sections/mouse/genotype. Bottom: cartoons summarizing IF data. *F*) Kcnq1 (red) and HKA β subunit (green). *G*) Kcnq1 (red) and NKCC (green). *H*) HKA β subunit (red) and NKCC (green). Width of view (except bottom merge): 100 μm (*F*); 75 μm (*G*, *H*).

this spectrum (15). Current-voltage relationships measured using patch clamp of transfected KCNQ1 alone or with KCNE2 in mammalian nonpolarized cell lines indicate that KCNE2 reduces the voltage dependence of KCNQ1 activation (11); however, in the crucial −20- to −40-mV range, homomeric KCNQ1 channels pass more current (in *e.g.*, 3-s pulses) at neutral pH than KCNE2–KCNQ1 complexes. While KCNQ1 channels are partially inhibited at low extracellular pH, KCNE2–KCNQ1 channel currents are increased; the former, however, still pass current even at pH 3, and low pH reduces homomeric KCNQ1 inactivation (16). The polarity of KCNQ1 trafficking would be expected to be fundamental to its role in PCs, and disruption of this trafficking an interesting candidate mechanism for the profound gastric effects produced by *Kcne2* deletion. However, previous studies failed to find any effects of KCNE subunits on KCNQ1 localization *in vitro* in Madin-Darby canine kidney (MDCK) cells (in which KCNQ1 remained basolateral regardless of coexpression with each of KCNE1–5) or *in vivo* in the colonic epithelium (in which KCNQ1 was basolateral in both wild-type and *Kcne3*$^{-/-}$ mice) (13, 17). Further, we recently discovered that KCNQ1–KCNE2 plays a crucial role in thyroid hormone biosynthesis, and that this channel appears to be basolaterally located in thyrocytes (18), contrasting with its apical localization in PCs. These apparent paradoxes, and the relative lack of understanding of the mechanisms underlying polarized trafficking of ion channels in general, prompted us to determine the effects of *Kcne* gene deletion on KCNQ1 trafficking in mouse PCs *in vivo*.

MATERIALS AND METHODS

Generation of gene-targeted mice

All mice used were housed and utilized according to the NIH Guide for the Care and Use of Laboratory Animals and Weill Medical College of Cornell University animal care and use policies. *Kcne2*$^{-/-}$ mice were generated as described previously from *Kcne2*$^{+/-}$ × *Kcne2*$^{+/-}$ crosses (2). *Kcne3* was disrupted through homologous recombination, using a targeting vector to replace the entire coding region, contained within the fourth exon, of the *Kcne3* gene. Two homologous arms, a 3.9-kb sequence homologous to the 5′ region upstream from exon 4 and a 3.0-kb sequence homologous to the 3′ downstream region, were subcloned into a pVBTk-loxP-knockout backbone vector. The vector contained a neomycin resistance (Neo_r) cassette flanked by LoxP sites, allowing for the removal of the cassette on expression of Cre-recombinase, and a TK^- selection marker (see **Fig. 4*A***). The targeting vector was linearized at a unique I-Ceu1 restriction enzyme site outside of the homologous region and electroporated into Albino C57BL/6 (C2J) ES cells. Clones were positively selected for Neo_r, and integration of the null vector was confirmed through Southern blot analysis with a 5′ probe directed at a 126-bp sequence located outside the recombined region. The probe was amplified by PCR using the following primers: forward 5′-GCAGAAGGTAGGCACTTGGG-3′ and reverse 5′-ACTGGGGGAGACAATAGGCG-3′. Correctly targeted ES cells were injected into C57BL/6 blastocysts and implanted into female mice, which were bred with C57BL/6 males to generate chimeric progeny of a 50:50 C57BL/6:Albino B6 (C2J) genetic background. Chimeras were interbred to produce *Kcne3*$^{+/-}$ mice. The *Kcne3*$^{-/-}$ mice used in this study were bred from *Kcne3*$^{+/-}$ × *Kcne3*$^{+/-}$ crosses.

To generate litters of *Kcne2*$^{+/-}$*Kcne3*$^{+/-}$ mice, male *Kcne2*$^{-/-}$ mice were bred with female *Kcne3*$^{-/-}$ mice. All double-heterozygous mice appeared superficially normal and were interbred to yield the *Kcne2*$^{-/-}$*Kcne3*$^{-/-}$ and *Kcne2*$^{+/-}$*Kcne3*$^{-/-}$ mice used in experiments. Genotyping for *Kcne2* was performed by PCR using the following oligonucleotide primers: 5′-CTGGAGGTAGCCAAATGGAGGAAG-3′, 5′-TCCTGCCAATC TTCCACGATGTAC-3′, and 5′-CGCTCCCGATTCGCAGCGCATC-3′, which generated a wild-type band of 382 bp and a knockout band of 680 bp. Genotyping for *Kcne3* was performed by PCR using the following oligonucleotide primers: 5′-CTATTCTACACG-CACTGTGGGATG-3′, 5′-CGTTGGAAGTCT CCATAGCAA-CAG-3′, and 5′-CGCTCCCGATTCGCAGCGCATC-3′, which generated a wild-type band of 280 bp and a knockout band of 1000 bp.

Quantitative RT-PCR (qRT-PCR)

Tissue extraction

Mice were euthanized by CO_2 asphyxiation. Stomachs were excised and washed in PBS, and the fundus was removed. Tissue was flash-frozen in liquid nitrogen and stored at −80°C until use. In preparation for RNA extraction, frozen tissue sections were submerged overnight or for 8 h in RNAlater Ice (Ambion, Austin, TX, USA) at −20°C.

RNA extraction

RNA was extracted from 30 mg of tissue with RNeasy Mini Kit (Qiagen, Valencia, CA, USA) according to the manufacturer's protocol. Tissue homogenization was achieved using a pestle grinder system (Fisher Scientific, Hampton, NH, USA). RNA yield and purity (A_{260}/A_{280}) were assessed by NanoDrop 2000 spectrophotometer (ThermoScientific, Waltham, MA, USA). RNA samples with A_{260}/A_{280} absorbance ratios between 1.80 and 2.10 were considered acceptable for cDNA synthesis.

cDNA synthesis

cDNA was synthesized from 1 μg of RNA with Quantitect Reverse Transcriptase (Qiagen) according to the manufacturer's protocol. To remove genomic DNA, template RNA was mixed with gDNA Wipeout Buffer (Qiagen) and incubated at 42°C for 2 min. Quantitect Reverse Transciptase containing an RNase inhibitor and Quantiscript RT Buffer containing Mg^{2+} and dNTPs were then added to the genomic DNA elimination reaction and incubated at 42°C for 15 min. The reverse transcription reaction was inactivated with a 3-min incubation at 95°C. Synthesized cDNA was analyzed immediately thereafter by qPCR or stored at −20°C until use.

Targeting information

qRT-PCR was conducted adhering as closely as possible to MIQE guidelines (19). Primer pairs for target gene *Kcne1* [National Center for Biotechnology Information (NCBI) GeneID 16509] produced an amplicon of 108 bp; match position of the expected sequence was number 1 out of 123 Basic Local Alignment Search Tool (BLAST; U.S. National

Institutes of Health, Bethesda, MD, USA) matches. Primer pairs for target gene *Kcne3* (NCBI GeneID 57442) produced an amplicon of 143 bp; match position of the expected sequence was number 1 out of 1001 BLAST matches. Primer pairs for target gene *Kcne4* (NCBI GeneID 57814) produced an amplicon of 126 bp. Primer pairs for target gene *Kcne5* (NCBI GeneID 66240) produced an amplicon of 113 bp; match position of the expected sequence was number 1 out of 428 BLAST matches. Primer pairs for reference gene *glyceraldehyde 3-phosphate dehydrogenase* (*GAPDH;* NCBI Gene ID 14433) produced an amplicon of 123 bp; match position of the expected sequence is number 1 out of 251 BLAST matches.

Primer information

Primer sequences for qPCR analysis were acquired from the Harvard Medical School PrimerBank (Boston, MA, USA; ref. 20) and were as follows: *Kcne1*, forward 5′-ATGAGCCTGCCCAATTCCAC-3′ and reverse 5′-GAGCTGAGACTTACGAGCCA-3′; *Kcne2*, forward 5′-CACATTAGCCAATTTGACCCAGA-3′ and reverse 5′-GAACATGCCGATCATCACCAT-3′; *Kcne3*, forward 5′-CTTTGCTCGATGGAAGGGGAC-3′ and reverse 5′-GCTGTCGTTGAGAGGCGTC-3′; *Kcne4*, forward 5′-CTGAGGATGGAGCCTCTGAAC-3′ and reverse 5′-AGCAAATCGAAACGAGTCCTTC-3′; *Kcne5*, forward 5′-AGATCCGCTGTCCTCCTCATT-3′ and reverse 5′-GGGTTCTGACCTCTCATCATCTT-3′; and *GAPDH*, forward 5′-AGGTCGGTGTGAACGGATTTG-3′ and reverse 5′-TGTAGACCATGTAGTTGAGGTCA-3′. Primers (50-nm synthesis scale, desalted) were acquired from Invitrogen (Carlsbad, CA, USA).

Assay details

qPCR analysis was performed on the Roche Light Cycler 480 System using LightCycler 480 SYBR Green I Master Mix and LightCycler 480 96-well white plates (Roche Diagnostics, Indianapolis, IN, USA). Each reaction contained ~75 ng of cDNA, 1 μl of PCR-grade water, 2 μl of 10 μM forward primer, 2 μl of 10 μM reverse primer, and 10 μl 2X Master Mix, which was comprised of dNTP mix, $MgCl_2$, FastStart *Taq*DNA Polymerase, reaction buffer, and SYBR Green I dye.

Cycling conditions

Thermocycling parameters were as follows: for amplification, 1 cycle at 95°C (10 min); 45 cycles at 95°C (5 s), 68°C (5 s), and 72°C (25 s); for melting curve, 95°C (1 s), 65°C (1 s), 95°C (continuous); for cooling, 1 cycle 45°C (15 s).

Data analysis

Advanced relative quantification was used to obtain normalized changes in expression levels of target genes (*Kcne1–5*) relative to controls (GAPDH) using LightCycler 480 1.5 software. Primer pairs were previously validated by PrimerBank with amplification plots, dissociation curves, and 2% agarose gel analysis. Primer pair amplification efficiency was also established with calibration curves within the laboratory on LightCycler 480 equipment, and deemed satisfactory for experimentation. The calibration curve for GAPDH yielded a slope of −3.334 and efficiency of 1.995. The calibration curve for *Kcne1* yielded a slope of −3.386 and efficiency of 1.974. The calibration curve for *Kcne3* yielded a slope of −3.362 and efficiency of 1.983. The calibration curve for *Kcne4* yielded a slope of −3.110 and efficiency of 2.097. The calibration curve for *Kcne5* yielded a slope of −3.315 and efficiency of 2.003. Each sample was run in triplicate as a quality control measure, and triplicates varying from one another by >1 cycle were discarded. Melting curves were assessed for each reaction to verify the amplification of a single product. Final analysis of statistical significance was calculated using 1-way analysis of variance (ANOVA) test (Origin).

Semiquantitative RT-PCR

The observation of *Kcne3* up-regulation in *Kcne2*$^{-/-}$ mouse fundus using qPCR was recapitulated using conventional semiquantitative RT-PCR on fundic cDNA, using different primer sequences to those used for qPCR, and an alternative reference gene: hypoxanthine-guanine phosphoribosyltransferase (HPRT). Briefly, RNA was extracted from 4 separate stomach fundi/genotype using an RNAeasy kit (Qiagen), then samples were diluted to give equal RNA concentrations, as assessed by spectrophotometry, before reverse-transcription to give cDNA as before (21). Primers used were as follows: *HPRT*, forward 5′-TGGAAAGAATGTCTTGATTGTTGA-3′ and reverse 5′-ACTTCGAGAGGTCCTTTTCACC-3′, which gives a 130-bp product; *Kcne3*, forward 5′-GGCTCTGAACACAACCCTTC-3′ and reverse 5′-TTTGTCCACTTTGCGTGAAC-3′, which gives a 205-bp product. Band densities of PCR products obtained with specific primers for HPRT transcript, run on a 1% agarose gel and stained with ethidium bromide, were measured using a Fluor-S MultiImager (Bio-Rad, Hercules, CA, USA) to confirm that the RNA-concentration-normalized samples each yielded similar amounts of this reference transcript. In parallel, cDNA samples from the same preps were amplified with *Kcne3*-specific primers, and optical density was measured. Results are expressed as mean optical density for each amplicon, with statistical analysis performed using 1-way ANOVA with statistical significance set at $P < 0.05$.

Immunostaining (IS) and immunofluorescence (IF)

KCNQ1 IS (Fig. 1*C–E*) was performed as we previously described (2). IF detection of HKA β, the $Na^+K^+2Cl^-$ cotransporter (NKCC1), KCNQ1, and KCNE3 was performed using a Discovery XT processor (Ventana Medical Systems, Tucson, AZ, USA). The primary antibody concentrations used were: 0.5 mg/ml anti-HKA β (mouse monoclonal; Affinity Bioreagents, Golden, CO, USA), 0.5 mg/ml anti-NKCC1 (goat polyclonal, Santa Cruz Biotechnology, Santa Cruz, CA, USA), and 1 mg/ml anti-KCNQ1 (rabbit or goat polyclonal; Chemicon, Temecula, CA, USA); in-house anti-KCNE3 serum was used at a 1:500 dilution after column-enriching IgG. Preceding the primary antibody incubation, the tissue sections were blocked for 30 min in 10% normal goat serum, 2% BSA in PBS, followed by 8 min avidin/biotin block. The primary antibody incubation (3 h) was followed by 32 min incubation with biotinylated anti-mouse IgG (Vectastain ABC kit; Vector Laboratories, Burlingame, CA, USA) for HKA β, 60 min incubation with biotinylated anti-goat IgG (Vectastain ABC kit) for NKCC1 (and for KCNQ1 for KCNE3 colocalization analysis), and biotinylated anti-rabbit or antibody at 1:200 dilution (Vectastain ABC kit) for KCNQ1 (for HKA and NKCC1 colocalization analysis). The secondary detection was performed with Streptavidin-HRP D (Ventana Medical Systems), followed by incubation with Tyramide-Alexa Fluor 488 (Invitrogen) or Tyramide Alexa Fluor 568 (Invitrogen). Stained slides were viewed with a Zeiss Axiovert 200 widefield microscope (Carl Zeiss, Oberkochen, Germany), and pictures were acquired using MetaMorph 7.1 software (Molecular Devices, Sunnyvale, CA, USA).

Western blotting and coimmunoprecipitation (co-IP)

For Western blotting, gastric membrane fractions were prepared as we previously described (2). Protein concentration of the supernatant was measured according to the Bradford method. Total protein (40 μg/lane) was loaded into a precast Tris-glycine 4–20% gel (Bio-Rad) and separated by electrophoresis. Proteins were then transferred onto a PVDF membrane (Bio-Rad) and blocked with 5% milk and 0.05% Tween-20 in PBS at 4°C on a rocker either for 1–2 h or overnight. Primary antibody incubations (4 h, room temperature, in 1% milk and 0.05% Tween-20 in PBS) were 1:1000 anti-KCNQ1 (Chemicon); 1:500 anti-KCNE3 (in-house anti-KCNE3 N terminus or anti-KCNE3 C terminus from Alomone Labs, Jerusalem, Israel); 1 mg/ml anti-NKCC1 (Santa Cruz Biotechnology). Membranes were washed 4 times, 20 min each, with antibody incubation buffer; incubated with the appropriate secondary antibodies (Bio-Rad), diluted 1:10,000 in buffer A, for 2 h at room temperature; then washed 4 times, 20 min each, with buffer A and once for 5 min with PBS. Membranes were incubated for 1 min with the SuperSignal ECL reagent (Pierce Biotechnology, Rockford, IL, USA), then exposed on BioMax Light Film (Kodak, Rochester, NY, USA) and developed using an RP X-OMAT processor (Kodak). For co-IPs, membrane fractions in buffer A—150 mM NaCl, 50 mM Tris-HCL (pH 7.4), 20 mM NaF, 10 mM $NaVO_4$, 1 mM phenylmethylsulfonyl fluoride (Fisher Scientific), 1% Nonidet P-40 (Pierce), 1% CHAPS (Sigma, St. Louis, MO, USA), 1% Triton X-100 (Fisher Scientific), and 0.5% SDS (Sigma)—were precleared with Protein A Sepharose beads (Amersham Bioscience), incubated with antibodies raised against KCNQ1 or NKCC1, and precipitated with Protein A Sepharose beads; then beads were washed with buffer A, and bound proteins were eluted with SDS-PAGE loading buffer for Western blotting as above.

Histology

For histology and stomach mass quantification, mice were killed using CO_2 asphyxiation (5–10/genotype). Stomachs and colons were removed postmortem, stomach mass was determined, and stomach and colon tissue was fixed in 10% neutral buffered formalin, processed by routine methods, and embedded in paraffin wax. Gastric mucosal and colonic epithelial sections were cut at 5-μm intervals, placed on positively charged Superfrost slides, stained with hematoxylin and eosin (H&E), and evaluated with an Olympus BX45 microscope (New York/New Jersey Scientific Inc., Middlebush, NJ, USA).

Whole-stomach pH measurements

Mice were killed by CO_2 asphyxiation. Stomachs were ligated *ex vivo* at the esophageal and duodenal junctures and excised. Stomachs were then incubated for 1 h in oxygenated HEPES-buffered Ringer's solution with or without 300 μM histamine (Sigma). After 1 h incubation time, stomach contents were aspirated, and pH was measured using a microcombination pH probe (Microelectrodes Inc., Bedford, NH, USA).

RESULTS AND DISCUSSION

Kcne2 deletion reverses the polarity of Kcnq1 trafficking in PCs

Having previously determined that Kcnq1 expression in the gastric mucosa is increased after targeted deletion of *Kcne2* (2), here we examined the effects of *Kcne2* deletion on the intracellular localization of Kcnq1 in PCs. In 3-mo-old $Kcne2^{-/-}$ mouse gastric mucosa, Kcnq1 IS demonstrated an apparent sharply basolateral localization in PCs across the mucosa, in contrast to its diffuse staining in $Kcne2^{+/+}$ PCs due to localization in the highly convoluted and invaginated apical membrane (Fig. 1*C–E*). Double IF staining confirmed that Kcnq1 was expressed in the apical side of PCs from 3-mo-old $Kcne2^{+/+}$ mice, colocalizing with the H^+/K^+ATPase β subunit (HKA β), a PC apical membrane marker, but not with NKCC1, a marker for basolateral membrane in PCs (22) (Fig. 1*F, G*). In contrast, in age-matched $Kcne2^{-/-}$ mouse gastric sections, Kcnq1 was still expressed in PCs (which were identified by midgastric gland location and HKA β expression), but was colocalized with NKCC1 at the PC basolateral membrane (Fig. 1*F, G*). HKA β was still expressed in the apical membrane of PCs, as described previously (23), and did not colocalize with NKCC1 in either $Kcne2^{+/+}$ or $Kcne2^{-/-}$ sections, demonstrating that *Kcne2* deletion did not globally disrupt PC polarity (Fig. 1*H*).

Kcne2 deletion selectively up-regulates fundic Kcne3

We considered two possible mechanisms underlying the observed switch in Kcnq1 location on *Kcne2* deletion: passive, arising from homomeric Kcnq1 trafficking to the basolateral membrane in the absence of a required chaperone (postulated to be Kcne2) to target its expression to the apical side; or active, due to hijacking by another Kcne subunit. We therefore next investigated possible Kcne remodeling in $Kcne2^{-/-}$ gastric fundus tissue, using qRT-PCR analysis of transcripts for each of the four remaining *Kcne* genes, with *GAPDH* serving as a reference gene. Strikingly, we observed that fundic *Kcne3* transcript expression was increased 3-fold at 3 mo of age by targeted deletion of *Kcne2* (n=10 mice/genotype; $P<0.05$), whereas there were no significant changes in the fundic expression of transcripts for *Kcne1*, *Kcne4*, or *Kcne5* (n=10 mice/genotype; $P > 0.4$) (**Fig. 2*A***). The observation that *Kcne3* mRNA was upregulated in $Kcne2^{-/-}$ fundus was recapitulated using conventional (semiquantitative) RT-PCR, with *HPRT* as a reference gene (n=4 mice/genotype; $P<0.01$; Fig. 2*B, C*). Notably, fundic Kcne3 protein expression was found to be increased 5-fold by *Kcne2* deletion (n=7 independent preps, 21–35 mice/genotype, $P<1\times10^{-4}$; Fig. 2*D, E*).

Kcne3 forms PC basolateral complexes with Kcnq1 in the absence of Kcne2

The fundic remodeling data (Fig. 2) suggested Kcne3 as the most likely Kcne candidate for diversion of Kcnq1 to the basolateral membrane in $Kcne2^{-/-}$ PCs. We adopted several biochemical and genetic approaches to test this hypothesis. First, we performed native co-IP studies using fundic tissue, and found greatly increased formation of Kcnq1–Kcne3 com-

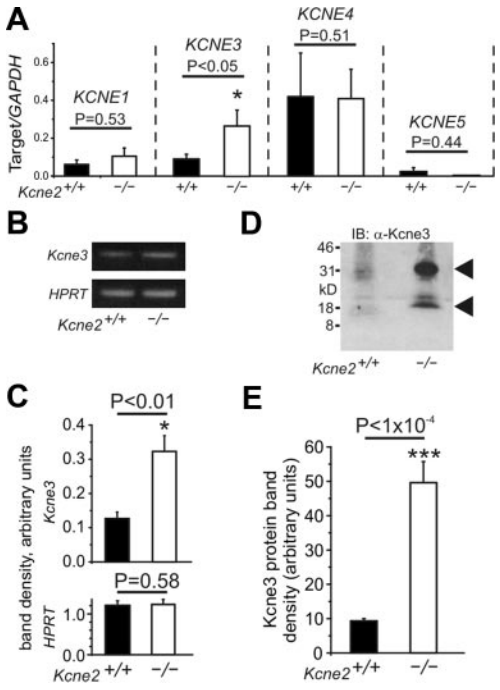

Figure 2. PC Kcne3 is selectively up-regulated in remodeling arising from targeted deletion of *Kcne2*. *A*) qRT-PCR analysis of remodeling of the fundic Kcne expression profile by targeted deletion of *Kcne2*; mRNA expression level expressed as a ratio to that of reference gene *GAPDH*; $n = 10$ mice/genotype/gene. *B*) Representative agarose gel of cDNA fragments for *Kcne3* and the reference gene *HPRT* after semi-quantitative RT-PCR from gastric mucosal lysates from $Kcne2^{+/+}$ and $Kcne2^{-/-}$ mice as indicated. *C*) Mean band optical densities from samples as in panel *B*; $n = 4$ independent preps (and mice)/genotype. *D*) Representative Western blot of Kcne3 protein in membrane fractions from $Kcne2^{+/+}$ and $Kcne2^{-/-}$ mouse fundus preparations as indicated, using anti-Kcne3 antibody. Migration distance of molecular mass markers is indicated at left. Arrows indicate expected sizes of nonglycosylated and fully glycosylated (mature) Kcne3. *E*) Band optical density from Kcne3 (mature form) Western blots of $Kcne2^{+/+}$ and $Kcne2^{-/-}$ gastric mucosal membrane fractions, as in panel *D*; $n = 7$ independent preparations from 3–5 stomachs each; total of 21–35 stomachs/genotype. Error bars = SEM.

plexes in $Kcne2^{-/-}$ tissue compared to $Kcne2^{+/+}$ tissue, with NKCC1 providing a negative control for Kcne3 co-IP (**Fig. 3*A***). These data were supported by IF analyses, which indicated increased Kcne3 expression compared to $Kcne2^{+/+}$ PCs, and basolateral colocalization of Kcne3 with Kcnq1, in $Kcne2^{-/-}$ PCs— similar to that observed in wild-type colonic epithelium (Fig. 3*B*).

Kcne3 is necessary and sufficient for trafficking of Kcnq1 to the PC basolateral membrane

These observations were suggestive of an active role for Kcne3 in rerouting Kcnq1 to the PC basolateral membrane, but it was still possible that Kcnq1 could target to the PC basolateral side regardless of Kcne3, in the absence of Kcne2. To resolve this, we generated $Kcne3^{-/-}$ mice by targeted deletion of the *Kcne3* gene (**Fig. 4*A***), and then crossed them with $Kcne2^{-/-}$ mice to generate heterozygous, and ultimately double-knock-

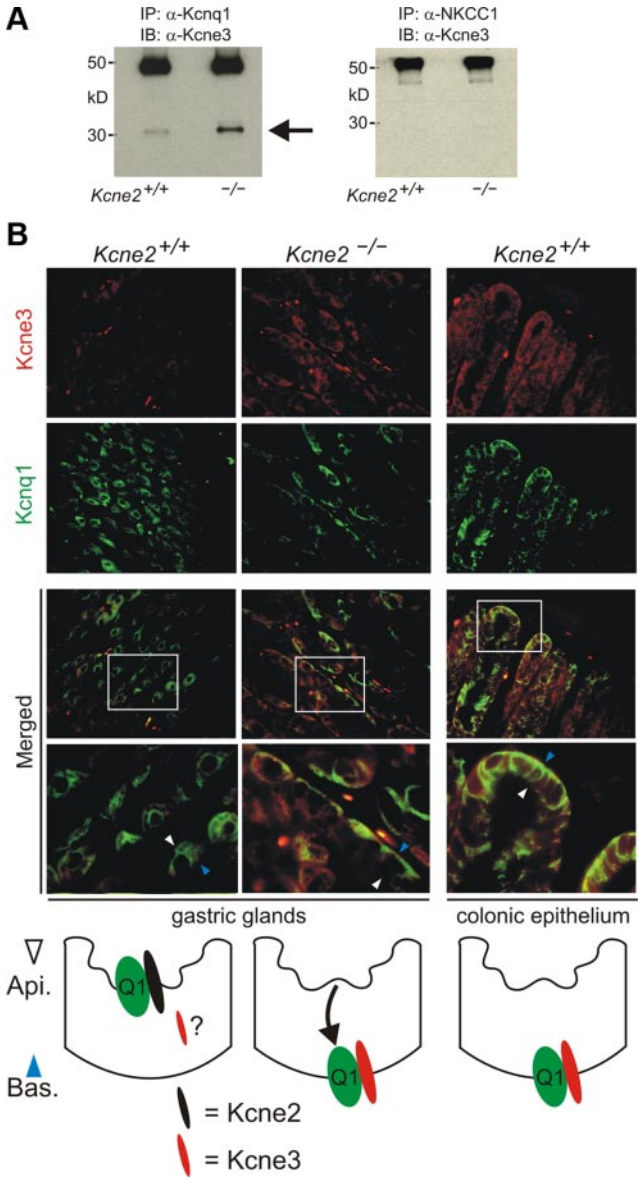

Figure 3. Remodeled Kcne3 forms basolateral complexes with Kcnq1 in $Kcne2^{-/-}$ PCs. *A*) Co-IPs showing complex formation of Kcne3 with Kcnq1 (left panel) but not with NKCC1 (right panel) from mouse fundic membrane fractions. IPs of fractions from $Kcne2^{+/+}$ and $Kcne2^{-/-}$ mice were prepared using antibodies raised against Kcnq1 or NKCC1, and Western blots were performed with anti-Kcne3 antibody. Numbers indicate migration of molecular mass markers (kDa). Arrow indicates expected mature Kcne3 migration distance. Top bands are precipitated antibodies. Representative of $n = 2$ experiments/antibody, with each prep pooled from 3–5 mouse stomachs/genotype. *B*) Top: exemplar IF labeling of Kcne3 (red) and Kcnq1 (green) in $Kcne2^{+/+}$ or $Kcne2^{-/-}$ gastric glands, or $Kcne2^{+/+}$ colonic crypts, as indicated. Merged panels show merged views of the 2 panels above; bottom merged panel shows expanded view of the boxed region in the top merged panel. Yellow indicates colocalization. Width of view (except bottom merge): 100 μm. Representative of results from at least two mice, 3–5 sections/mouse/genotype. Bottom: cartoons summarizing IF data.

out, *Kcne2*$^{-/-}$*Kcne3*$^{-/-}$ mice. We confirmed their genotypes with PCR (Fig. 4*B*) and with Western blots from colon tissue, in which Kcne3 is known to be expressed (10) (Fig. 4*C*). Next, we determined whether there was remodeling of *Kcne1*, *Kcne4*, or *Kcne5* due to concomitant *Kcne2* and *Kcne3* deletion, again using qRT-PCR. These experiments did not identify statistically significant changes in mRNA expression of these 3 genes; there was a general trend toward reduced expression, but considerable variability in expression within each genotype (Fig. 4*D*). Strikingly, IF studies showed that Kcnq1 colocalized in the apical compartment with HKA β, and not basolaterally with NKCC1, in *Kcne2*$^{-/-}$ *Kcne3*$^{-/-}$ mouse PCs (Fig. 4*E*, *F*). As we might have expected, Kcnq1 was also apically expressed in *Kcne2*$^{+/+}$ *Kcne3*$^{-/-}$ mouse PCs (Fig. 4*E*, *F*). Thus, in PCs, Kcne2 is not required for apical localization of Kcnq1 in the absence of Kcne3. However, in the absence of Kcne2, Kcne3 is up-regulated and is necessary and sufficient to actively chaperone Kcnq1 to the PC basolateral membrane.

Kcne2 is required for Kcnq1 *function* at the PC apical membrane

Our findings suggested that in *Kcne2*$^{-/-}$*Kcne3*$^{+/+}$ mouse PCs, Kcnq1–Kcne3 channels could form an additional basolateral K^+ efflux route, but that there would be no apical K^+ recycling pathway. In contrast, in *Kcne2*$^{-/-}$*Kcne3*$^{-/-}$ mouse PCs, homomeric Kcnq1 could potentially provide an apical K^+ recycling pathway, but in the absence of Kcne2 its functionality might be limited, due to an inability to function efficiently at low pH and/or negative membrane potentials. There are several hypothetical consequences of these mistrafficking and subunit rearrangement events. Basolateral Kcnq1–Kcne3 channels in *Kcne2*$^{-/-}$*Kcne3*$^{+/+}$ mice could potentially restore some gastric acid secretion by alleviating PC K^+ accumulation. In contrast, *Kcne2*$^{-/-}$ *Kcne3*$^{-/-}$ mice would exhibit restored gastric acidification if Kcnq1 was able to function alone at the apical membrane, but if homomeric Kcnq1 did not have this capability, *Kcne2*$^{-/-}$*Kcne3*$^{-/-}$ mice would potentially have the most severe gastric pathology of all the genotypes. *Kcne2*$^{+/+}$*Kcne3*$^{-/-}$ mice would be predicted to have normal gastric acidification.

We tested these hypotheses by measuring stomach mass to quantify gastric hyperplasia (one consequence of achlorhydria), and by quantifying gastric luminal pH. These studies yielded the striking finding that Kcne3 indeed affected gastric function and cell proliferation in *Kcne2*-depeleted mice, but not in mice with both *Kcne2* alleles. Thus, 3-mo-old *Kcne2*$^{-/-}$*Kcne3*$^{-/-}$ mice exhibited massive gastric hyperplasia, with twofold heavier stomachs than age-matched *Kcne2*$^{-/-}$*Kcne3*$^{+/+}$ mice, whereas *Kcne2*$^{+/+}$*Kcne3*$^{-/-}$ mice had normal stomach mass (Fig. 5*A*, *B*). Notably, Kcne3 also prevented gastric hyperplasia in *Kcne2*$^{+/-}$*Kcne3*$^{+/+}$ mice, which had significantly smaller stomachs than those of *Kcne2*$^{+/-}$*Kcne3*$^{-/-}$ mice (Fig. 5*B*). These data were supported by results from stomach lumen pH quantification, which indicated that *Kcne2*$^{+/-}$*Kcne3*$^{-/-}$ mice had significantly less gastric acidification upon histamine stimulation than *Kcne2*$^{+/-}$*Kcne3*$^{+/+}$ mice, although Kcne3 did not affect the stomach lumen pH or response to histamine of *Kcne2*$^{-/-}$ mice. As expected, *Kcne2*$^{+/+}$*Kcne3*$^{-/-}$ mice had normal stomach pH and response to histamine (Fig. 5*C*).

These findings are consistent with a novel model in which, in the absence of Kcne2, Kcne3 is upregulated and chaperones Kcnq1 to the PC basolateral side. When both *Kcne3* and *Kcne2* are deleted, homomeric Kcnq1 localizes to the apical membrane, but without restoration of gastric acidification. This indicates that Kcnq1 cannot function in the absence of both Kcne2 and Kcne3 in PCs, even if at the apical membrane, due either to inhibition by low extracellular pH, inability to constitutively activate, or both (Fig. 5*D*).

Implications of Kcne-directed polarized trafficking of Kcnq1

This study describes two main novel findings: discovery of the capacity of a KCNE subunit to act as a polar trafficking chaperone, and identification of KCNE subunit remodeling (and its functional consequences) *in vivo*. In native PCs, Kcnq1 probably localizes primarily in deeply invaginated sections of the apical membrane both at rest and when stimulated, although a fraction of it may be located in intracellular vesicles and move to the apical surface on secretagogue stimulation; in contrast, HKA is primarily located in intracellular vesicles until stimulation triggers its trafficking to the apical membrane (16, 24). Here, we show that *Kcne2* deletion results in Kcnq1 residing basolaterally in PCs instead, and that Kcne3 is necessary and sufficient for this rerouting. In a previous study of MDCK cells, Kcnq1 was basolaterally located regardless of which Kcne subunit (subunits 1 through 5) it was heterologously coexpressed with (17), and we recently found that Kcnq1–Kcne2 channels are basolaterally located in thyrocytes (18). Furthermore, Kcne3 does not appear necessary for basolateral location of Kcnq1 in colonic epithelium, although potential remodeling of other Kcne subunits was not determined in that study (13). Clearly, the influence of Kcne subunits on Kcnq1 targeting in polarized cells is highly cell-type specific, perhaps due to differences in expression of proteins such as μ1B, an AP-1 clathrin adaptor complex that directs polarized trafficking (25–27).

The discovery of Kcne remodeling due to genetic disruption of another Kcne subunit has potentially profound implications for the etiology of Kcne-related disease states and for study of *Kcne*-knockout mice. In previous studies examining K^+ channel α subunit gene deletion, a concern has been that functional redundancy exists given the similarity of some α subunits, *e.g.*, Kv3.1 and Kv3.2 (28). Here, studying β subunits, we have unearthed a novel remodeling phenomenon, wherein the location of the α subunit in the absence of

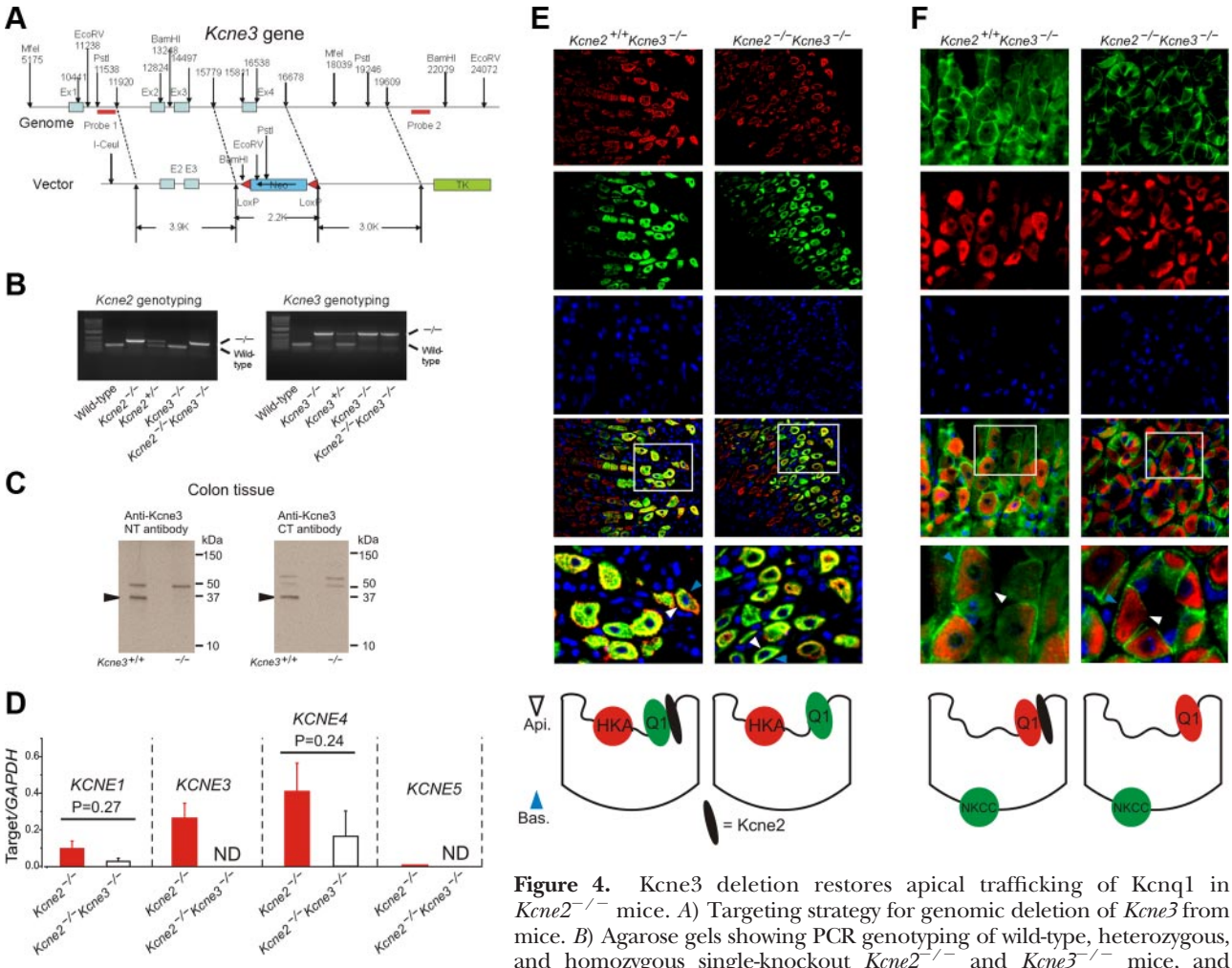

Figure 4. Kcne3 deletion restores apical trafficking of Kcnq1 in *Kcne2*$^{-/-}$ mice. *A*) Targeting strategy for genomic deletion of *Kcne3* from mice. *B*) Agarose gels showing PCR genotyping of wild-type, heterozygous, and homozygous single-knockout *Kcne2*$^{-/-}$ and *Kcne3*$^{-/-}$ mice, and double-knockout *Kcne2*$^{-/-}$*Kcne3*$^{-/-}$ mice. *C*) Western blots of Kcne3 protein in membrane fractions from colonic crypts of *Kcne3*$^{+/+}$ and *Kcne3*$^{-/-}$ mice as indicated, using an in-house antibody raised against a Kcne3 N-terminal epitope (left panel), and a commercial antibody (Alomone) raised against a Kcne3 C-terminal epitope (right panel). Migration distance of molecular mass markers is indicated at right. Arrows indicate band at 37 kDa unique to wild-type tissue. *D*) qRT-PCR analysis of remodeling of the fundic *Kcne* expression profile by targeted deletion of both *Kcne2* and *Kcne3*; expression level expressed as a ratio to that of reference gene GAPDH amplified in parallel each time; $n = 10$ mice/single gene deletion genotype; $n = 5$ mice/double gene deletion genotype. ND, not determined (for *Kcne3*, not measured in *Kcne2*$^{-/-}$*Kcne3*$^{-/-}$ mice; for *Kcne5*, unable to detect signal conforming to quality controls as described in Materials and Methods). Error bars = SEM. *E, F*) Top: exemplar IF colabeling of *Kcne2*$^{+/+}$ *Kcne3*$^{-/-}$ and *Kcne2*$^{-/-}$*Kcne3*$^{-/-}$ gastric glands as indicated. Bottom two IF panels are merged views of the 3 panels above; bottom merged panel shows expanded view of the boxed region in the top merged panel. Blue arrowheads, PC basolateral side; white arrowheads, PC apical side. Counterstained with DAPI (blue). Representative results from ≥2 mice, 3–5 sections/mouse/genotype. Bottom: cartoons summarizing IF data. *E*) Kcnq1 (green) and HKA β subunit (red). *F*) Kcnq1 (red) and NKCC1 (green). Width of view (except bottom merge): 100 μm (*E*); 50 μm (*F*).

its regular β subunit partner is the polar opposite of that observed in wild-type mice—due to hijacking by a remodeled (upregulated), related β subunit. We suspect we have merely scratched the surface with respect to the prevalence of Kcne subunit remodeling in both model systems and in animal and human disease states in a variety of tissues, a hypothesis to be tested further in the future. The present findings highlight the importance not only of an apical localization *per se* for Kcnq1, but also the association with Kcne2 for full functionality at the apical side. Kcnq1–Kcne3 channels are acid-insensitive (29) and, like Kcnq1–Kcne2, are constitutively active, so one would assume they could provide an apical K^+ recycling conduit if located there, but they could not rescue gastric acid secretion in *Kcne2*$^{-/-}$ mice because they were basolaterally located in parietal cells, although they partially restored function in *Kcne2*$^{+/-}$ mice. By the same token, even when apically located, Kcnq1 could not serve as a K^+ recycling channel without Kcne2 in PCs—we speculate this is because homomeric Kcnq1 is voltage dependent and inhibited by acid. Our data suggest that Kcnq1 defaults to the apical side in the absence of Kcne2 or Kcne3, but further studies are required, perhaps adopting a proteomic approach together with the genetic models described here, to determine whether Kcnq1 requires an additional subunit to traffic apically in parietal cells, which is either upregulated on Kcne2 and Kcne3 double knockout, or simply permitted to associate with Kcnq1 only in the absence of these subunits. The

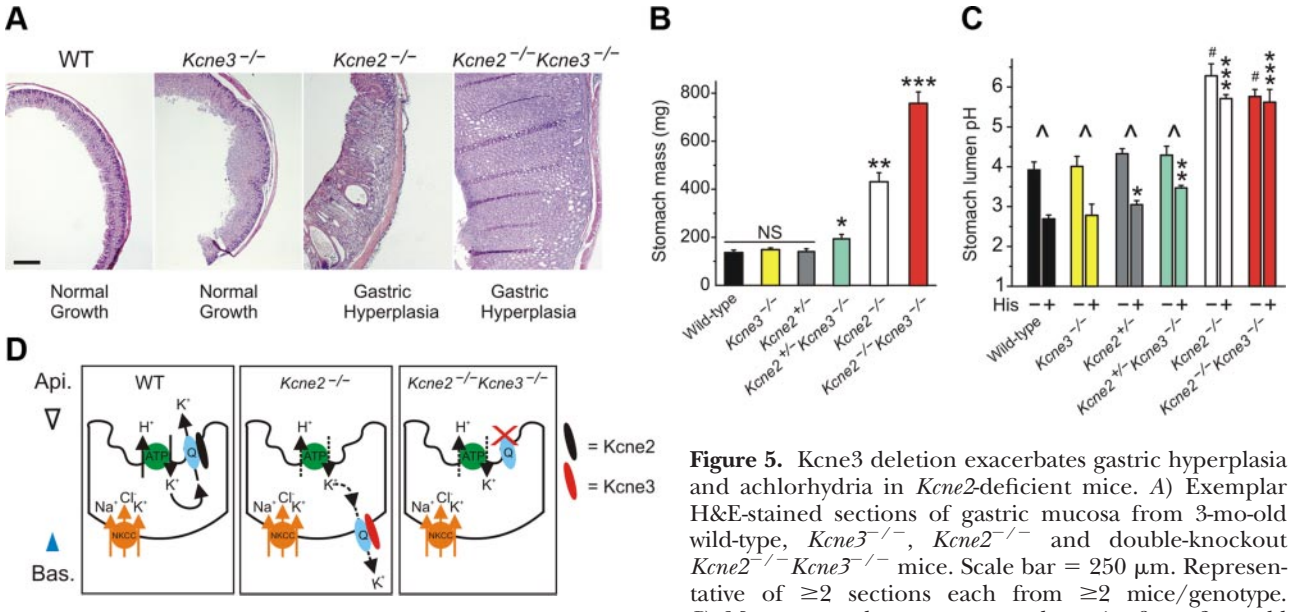

Figure 5. Kcne3 deletion exacerbates gastric hyperplasia and achlorhydria in *Kcne2*-deficient mice. *A*) Exemplar H&E-stained sections of gastric mucosa from 3-mo-old wild-type, $Kcne3^{-/-}$, $Kcne2^{-/-}$ and double-knockout $Kcne2^{-/-}Kcne3^{-/-}$ mice. Scale bar = 250 μm. Representative of ≥2 sections each from ≥2 mice/genotype. *B*) Mean stomach mass measured *ex vivo* from 3-mo-old mice, genotypes as indicated, $n = 6$–16. NS, nonsignificant. $^{*}P < 0.05$; $^{**}P < 2 \times 10^{-4}$; $^{***}P < 4 \times 10^{-5}$. *C*) Mean stomach lumen pH measured *ex vivo* from 3-mo-old mice, genotypes as indicated, with (+) or without (−) stimulation with 300 μM histamine (His); $n = 3$–5. $^{*}P < 0.05$, $^{**}P < 0.03$, $^{***}P < 0.002$ *vs.* all other His groups; $^{\#}P < 0.01$ *vs.* all other control groups; $^{\wedge}P < 0.05$ *vs.* corresponding control group. *D*) Summary illustrating Kcne control of Kcnq1 trafficking in mouse PCs. Error bars = SEM.

mechanism underlying basolateral trafficking of Kcnq1–Kcne3 complexes in parietal cells is likely both Kcne3 and parietal cell dependent, and its elucidation will require use of chimeric Kcne subunits introduced either *in vivo* or into a suitable polarized parietal cell line; the former is more attractive because physiological consequences would be readily assayable. Our co-IP data suggest some (albeit relatively low-level) formation of Kcnq1–Kcne3 complexes even in wild-type gastric epithelium, which could correspond to complexes in gastric surface cells, or in chief cells, two gastric mucosal cell types suggested to express basolateral Kcnq1 and Kcne3; these cells are not located midgastric gland and do not express Kcne2 or HKA, and thus are easily distinguishable from PCs in IF studies (13, 29). Alternatively, Kcnq1–Kcne3 complexes could be occurring even in wild-type PCs, again albeit at relatively low levels. Further studies will identify what if any function these putative channels perform in PCs, and whether or not these are actually mixed Kcnq1–Kcne2–Kcne3 complexes, perhaps with functional characteristics we do not yet understand. This type of tripartite complex has been reported for Kcne1, Kcne3, and Kcnh3 in mouse brain (30).

Future work will determine which Kcne subunits or other factors control polarized trafficking of Kcnq1 in, *e.g.*, the thyroid, and of other α subunits in polarized cells in general, together with a search for the molecular signals that cause, *e.g.*, *Kcne3* transcript up-regulation in $Kcne2^{-/-}$ mouse PCs. The extent to which perturbation of this polarized trafficking contributes directly to, or is reflective of compensatory remodeling in, the molecular etiology of human diseases of the epithelia and other related systems, will be explored—particularly in the light of our recent finding that $Kcne2^{-/-}$ mice develop gastritis cystica profunda and gastric neoplasia (31). FJ

The authors are grateful for expert technical assistance from S. Backovic, L. Cohen-Gould (Director of the Electron Microscopy and Histology Core Facility at Weill Cornell Medical College), M. S. Jiao, the Molecular Cytology Core Facility of Memorial Sloan-Kettering Cancer Center, Sloan-Kettering Institute Mouse Genetics Core Facility, and Rockefeller University Transgenic Mouse Facility. G.W.A. is thankful for support from the National Heart, Lung, and Blood Institute; the National Institutes of Health (NIH; R01 HL079275); the American Heart Association (grant-in-aid 0855756D); and an Irma T. Hirschl Career Scientist Award. K.P. is supported by an NIH predoctoral training grant (T32GM073546).

REFERENCES

1. Lee, M. P., Ravenel, J. D., Hu, R. J., Lustig, L. R., Tomaselli, G., Berger, R. D., Brandenburg, S. A., Litzi, T. J., Bunton, T. E., Limb, C., Francis, H., Gorelikow, M., Gu, H., Washington, K., Argani, P., Goldenring, J. R., Coffey, R. J., and Feinberg, A. P. (2000) Targeted disruption of the Kvlqt1 gene causes deafness and gastric hyperplasia in mice. *J. Clin. Invest.* **106,** 1447–1455
2. Roepke, T. K., Anantharam, A., Kirchhoff, P., Busque, S. M., Young, J. B., Geibel, J. P., Lerner, D. J., and Abbott, G. W. (2006) The KCNE2 potassium channel ancillary subunit is essential for gastric acid secretion. *J. Biol. Chem.* **281,** 23740–23747
3. Fujita, A., Horio, Y., Higashi, K., Mouri, T., Hata, F., Takeguchi, N., and Kurachi, Y. (2002) Specific localization of an inwardly rectifying K(+) channel, Kir4.1, at the apical membrane of rat gastric parietal cells; its possible involvement in K(+) recycling for the H(+)-K(+)-pump. *J. Physiol.* **540,** 85–92
4. Malinowska, D. H., Sherry, A. M., Tewari, K. P., and Cuppoletti, J. (2004) Gastric parietal cell secretory membrane contains PKA- and acid-activated Kir2.1 K+ channels. *Am. J. Physiol. Cell Physiol.* **286,** C495–C506
5. Barhanin, J., Lesage, F., Guillemare, E., Fink, M., Lazdunski, M., and Romey, G. (1996) K(V)LQT1 and lsK (minK) proteins

associate to form the I(Ks) cardiac potassium current. *Nature* **384,** 78–80
6. Sanguinetti, M. C., Curran, M. E., Zou, A., Shen, J., Spector, P. S., Atkinson, D. L., and Keating, M. T. (1996) Coassembly of K(V)LQT1 and minK (IsK) proteins to form cardiac I(Ks) potassium channel. *Nature* **384,** 80–83
7. Abbott, G. W., Sesti, F., Splawski, I., Buck, M. E., Lehmann, M. H., Timothy, K. W., Keating, M. T., and Goldstein, S. A. (1999) MiRP1 forms IKr potassium channels with HERG and is associated with cardiac arrhythmia. *Cell* **97,** 175–187
8. McCrossan, Z. A., and Abbott, G. W. (2004) The MinK-related peptides. *Neuropharmacology* **47,** 787–821
9. Panaghie, G., and Abbott, G. W. (2007) The role of S4 charges in voltage-dependent and voltage-independent KCNQ1 potassium channel complexes. *J. Gen. Physiol.* **129,** 121–133
10. Schroeder, B. C., Waldegger, S., Fehr, S., Bleich, M., Warth, R., Greger, R., and Jentsch, T. J. (2000) A constitutively open potassium channel formed by KCNQ1 and KCNE3. *Nature* **403,** 196–199
11. Tinel, N., Diochot, S., Borsotto, M., Lazdunski, M., and Barhanin, J. (2000) KCNE2 confers background current characteristics to the cardiac KCNQ1 potassium channel. *EMBO J.* **19,** 6326–6330
12. Dedek, K., and Waldegger, S. (2001) Colocalization of KCNQ1/KCNE channel subunits in the mouse gastrointestinal tract. *Pflügers Arch.* **442,** 896–902
13. Preston, P., Wartosch, L., Gunzel, D., Fromm, M., Kongsuphol, P., Ousingsawat, J., Kunzelmann, K., Barhanin, J., Warth, R., and Jentsch, T. J. (2010) Disruption of the K+ channel beta-subunit KCNE3 reveals an important role in intestinal and tracheal Cl- transport. *J. Biol. Chem.* **285,** 7165–7175
14. Vallon, V., Grahammer, F., Volkl, H., Sandu, C. D., Richter, K., Rexhepaj, R., Gerlach, U., Rong, Q., Pfeifer, K., and Lang, F. (2005) KCNQ1-dependent transport in renal and gastrointestinal epithelia. *Proc. Natl. Acad. Sci. U. S. A.* **102,** 17864–17869
15. Okada, Y., and Ueda, S. (1984) Electrical membrane responses to secretagogues in parietal cells of the rat gastric mucosa in culture. *J. Physiol.* **354,** 109–119
16. Heitzmann, D., Grahammer, F., von Hahn, T., Schmitt-Graff, A., Romeo, E., Nitschke, R., Gerlach, U., Lang, H. J., Verrey, F., Barhanin, J., and Warth, R. (2004) Heteromeric KCNE2/KCNQ1 potassium channels in the luminal membrane of gastric parietal cells. *J. Physiol.* **561,** 547–557
17. Jespersen, T., Rasmussen, H. B., Grunnet, M., Jensen, H. S., Angelo, K., Dupuis, D. S., Vogel, L. K., Jorgensen, N. K., Klaerke, D. A., and Olesen, S. P. (2004) Basolateral localisation of KCNQ1 potassium channels in MDCK cells: molecular identification of an N-terminal targeting motif. *J. Cell Sci.* **117,** 4517–4526
18. Roepke, T. K., King, E. C., Reyna-Neyra, A., Paroder, M., Purtell, K., Koba, W., Fine, E., Lerner, D. J., Carrasco, N., and Abbott, G. W. (2009) Kcne2 deletion uncovers its crucial role in thyroid hormone biosynthesis. *Nat. Med.* **15,** 1186–1194
19. Bustin, S. A., Benes, V., Garson, J. A., Hellemans, J., Huggett, J., Kubista, M., Mueller, R., Nolan, T., Pfaffl, M. W., Shipley, G. L., Vandesompele, J., and Wittwer, C. T. (2009) The MIQE guidelines: minimum information for publication of quantitative real-time PCR experiments. *Clin. Chem.* **55,** 611–622
20. Spandidos, A., Wang, X., Wang, H., Dragnev, S., Thurber, T., and Seed, B. (2008) A comprehensive collection of experimentally validated primers for polymerase chain reaction quantitation of murine transcript abundance. *BMC Genomics* **9,** 633
21. Roepke, T. K., Kontogeorgis, A., Ovanez, C., Xu, X., Young, J. B., Purtell, K., Goldstein, P. A., Christini, D. J., Peters, N. S., Akar, F. G., Gutstein, D. E., Lerner, D. J., and Abbott, G. W. (2008) Targeted deletion of kcne2 impairs ventricular repolarization via disruption of I(K,slow1) and I(to,f). *FASEB J.* **22,** 3648–3660
22. McDaniel, N., Pace, A. J., Spiegel, S., Engelhardt, R., Koller, B. H., Seidler, U., and Lytle, C. (2005) Role of Na-K-2Cl cotransporter-1 in gastric secretion of nonacidic fluid and pepsinogen. *Am. J. Physiol. Gastrointest. Liver Physiol.* **289,** G550–G560
23. Courtois-Coutry, N., Roush, D., Rajendran, V., McCarthy, J. B., Geibel, J., Kashgarian, M., and Caplan, M. J. (1997) A tyrosine-based signal targets H/K-ATPase to a regulated compartment and is required for the cessation of gastric acid secretion. *Cell* **90,** 501–510
24. Kaufhold, M.-A., Krabbenhoft, A., Song, P., Engelhardt, R., Riederer, B., Fahrmann, M., Klocker, N., Biel, W., Manns, M., Hagen, S. J., and Seidler, U. (2008) Localization, trafficking, and significance for acid secretion of parietal cell Kir4.1 and KCNQ1 K+ channels. *Gastroenterology* **134,** 1058–1069
25. Matter, K., Hunziker, W., and Mellman, I. (1992) Basolateral sorting of LDL receptor in MDCK cells: the cytoplasmic domain contains two tyrosine-dependent targeting determinants. *Cell* **71,** 741–753
26. Odorizzi, G., Pearse, A., Domingo, D., Trowbridge, I. S., and Hopkins, C. R. (1996) Apical and basolateral endosomes of MDCK cells are interconnected and contain a polarized sorting mechanism. *J. Cell Biol.* **135,** 139–152
27. Duffield, A., Folsch, H., Mellman, I., and Caplan, M. J. (2004) Sorting of H,K-ATPase beta-subunit in MDCK and LLC-PK cells is independent of mu 1B adaptin expression. *Traffic* **5,** 449–461
28. Porcello, D. M., Ho, C. S., Joho, R. H., and Huguenard, J. R. (2002) Resilient RTN fast spiking in Kv3.1 null mice suggests redundancy in the action potential repolarization mechanism. *J. Neurophysiol.* **87,** 1303–1310
29. Heitzmann, D., and Warth, R. (2008) Physiology and pathophysiology of potassium channels in gastrointestinal epithelia. *Physiol. Rev.* **88,** 1119–1182
30. Clancy, S. M., Chen, B., Bertaso, F., Mamet, J., and Jegla, T. (2009) KCNE1 and KCNE3 beta-subunits regulate membrane surface expression of Kv12.2 K(+) channels in vitro and form a tripartite complex in vivo. *PLoS ONE* **4,** e6330
31. Roepke, T. K., Purtell, K., King, E. C., La Perle, K. M., Lerner, D. J., and Abbott, G. W. (2010) Targeted deletion of Kcne2 causes gastritis cystica profunda and gastric neoplasia. *PLoS ONE* **5,** e11451

Received for publication October 2, 2010.
Accepted for publication October 28, 2010.